Development and evaluation of mechanistic models for predicting the PET image quality of EGFR-TKIs in NSCLC patients

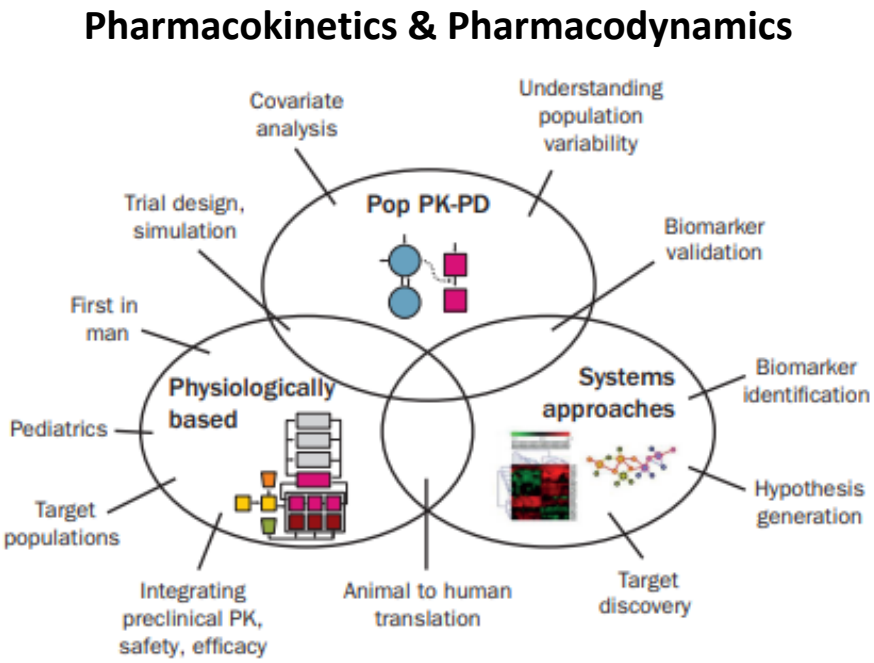

Author: Jemayro Hupsel (5681979)

Supervisor: Dr. I.H. Bartelink

Referee: Prof. Dr. N.H. Hendrikse

Examiner: Ewoudt van de Garde

Date: 15-04-2022

Version: 3.1

Amsterdam UMC
Universitair Medische Centra

Universiteit Utrecht

Abstract

Introduction: Epidermal growth factor receptor (EGFR) tyrosine kinase inhibitor (TKIs) are standard of care in EGFR-postive NSCLC patients. The issue uptake of NSCLC can be determined using radiolabeled EGFR TKI PET/CT. However, recent research has shown a significant difference between image quality (i.e. tumor-to-lung contrast) in in three generation EGFR TKIs: ^{11}C-erlotinib, ^{18}F-afatinib and ^{11}C-osimertinib. In this research we aim to develop a mechanistical model to predict the tumor-to-lung contrast and uptake of healthy tissue of the three tracers.

Methods: Relevant physicochemical & drug specific properties (e.g. pKa, lipophilicity, EGFR binding) for each TKI were collected and used in established base models. Key hallmarks of NSCLC: immune tumor deprivation, unaltered tumor perfusion and erratic neovascularization. Analysis was performed by excluding each key component and comparing the PE with the final mechanistical PBPK-model predictions. Model accuracy was demonstrated by calculating the prediction error (PE) between predicted tissue to blood ratios (TBR) and measured, PET image derived, TBR.

Results: The fitted models were able to predict the tumor-to-lung contrast for all EGFR-TKIs within 3-fold of observed PET image ratios (PE Tumor-to-lung ratio of -93%, +43% and-7.4 % for erlotinib, osimertinib and afatinib respectively). Furthermore, the models depicted agreeable whole-body distribution for osimertinib and afatinib, showing high tissue distribution and an underprediction and low tissue distribution at high blood concentrations for erlotinib (mean PE, of -4.4%, range -156% - +187%, for all tissues).

Conclusion: The developed models adequately predicted the image quality of afatinib, osimertinib and erlotinib. Some deviations in predicted whole-body TBR lead to new hypotheses such increased affinity for mutated EGFR and active influx transport (erlotinib into excreting tissues) or active efflux (afatinib from brain), which is currently unaccounted for. In the future, the models may be used to predict the image quality of new tracers.

Inhoud

Introduction

Lung cancer is the main cause of cancer-related mortality worldwide, with an estimation of 1.8 million deaths and over 2 million new cases each year [1]. Over the past decades treatment of non-small cell lung cancer (NSCLC) has changed from chemotherapy to more effective and better tolerated targeted therapies against specific oncogenic driver pathways [2]. An important one is the epidermal growth factor receptor (EGFR) pathway [3]. EGFR is a receptor tyrosine kinase that dimerizes, auto-phosphorylates and initiates a downstream signalling cascade [4]. An activating mutation in the kinase domain of the receptor can lead to ligand-independent activation [5,6]. EGFR tyrosine kinase inhibitors (TKIs) inhibit the intracellulair ATP-bindingpocket in the kinase domain [3,7]. Overexpression and activating mutations in EGFR predict response to specific TKIs in NSCLC patients [5,6]. Currently, three generations of EGFR-TKIs are approved for the treatment of EGFR mutation-positive NSCLC **(Figure 1).** The first-generation, in this study represented by erlotinib, binds reversibly to EGFR harboring mutations and to a lesser extent to wild-type EGFR [3,7,8]. To overcome resistant mutations, second-generation TKIs represented by afatinib were developed. However, the efficacy on the T790M mutation was unstatisfactory [7]. To achieve a more potent binding to the T790M mutation, 3rd generation TKIs, represented by osimertinib, were developed. An added benefit was that it has a reduced activity against wild-type EGFR [9]. Overall, treatment using EGFR-TKIs has shown better response rates and longer durations of response. As a result it has become standard of care in EGFR mutation-positive NSCLC patients [1].

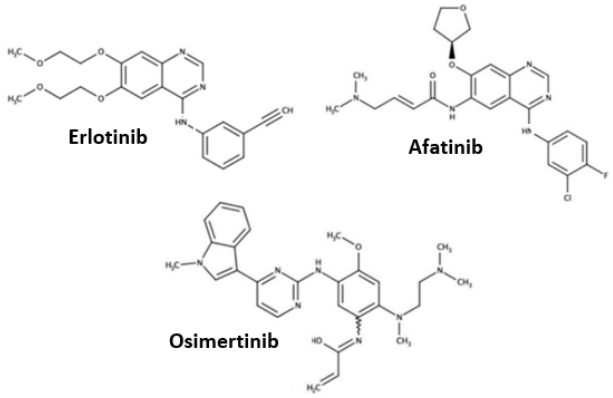

Figure 1: The chemical structure of three generations of EGFR-TKIs. The first generation represented by erlotinib, the second by afatinib and the third bij osimertinib [10].

In the last few years, research has been conducted using positron emission tomography (PET) to explore drug uptake as a predictive biomarker for response to EGFR-TKI treatment. The three generations of EGFR-TKI were radiolabeledand and the uptake was studied in patients exposed to 11C-erlotinib, 18F-afatinib and 11C-osimertinib. These PET tracers can be used to predict whole-body and tumor drug uptake [11-16]. In a recent study, published data from NSCLC patient scans of the three tracers was compared and analyzed, tracer uptake was quantified using the tumor-to-blood ratio (TBR) [17]. Previous research has shown that the TBR is an adequate measure for quantification of TKI-tracer uptake [15-17]. It was calculated by dividing tissue standard uptake value (SUV) by blood pool SUV [15]. The SUV is the standardized unit of semiquantitive analysis of PET-imaging. Furthermore, tumor visibility on the PET image in contrast to lung visibility, known as tumor-to-long contrast, was used to assess the PET image quality of each tracer. A difference in contrast was observed. 11C-osimertinib showed a negative contrast: tumor tissue uptake was 20% lower than surrounding lung tissue. Conversely, 18F-afatinib showed a 96% higher uptake in tumor tissue than in surrounding tissue. 11C-erlotinib image quality was deemed superior, with a tumor-to-lung contrast value of 178%. The three TKIs showed image quality ranking that was not explicable by physiochemical ranking. No reason for the difference in image quality has been found yet [17].

van de Stadt et al. hypothesized that physiochemical drug properties may explain the variability in penetration of the tracers in different tissues and between TKIs [17]. Properties that are ought to be relevant are acidity (defined by the pKa), lipophilicity (log P), albuminbinding and blood/plasma ratio (B:P) (**Table 1**). These

properties affect the tissue uptake in different ways. Firstly, a strong basic drug (pKa ≥ 7), is highly protonated at physiological (plasma) pH levels, whereas weak bases (pKa <7) are mostly unprotonated at physiological pH levels [18]. Protonation also affects transport over membranes. A protonated base, and thus ionized, will not pass the membrane passively without a carrier. Secondly, Lipophilicity affects tissue penetration. Strong lipophilic bases tend to diffuse to a greater extent [18]. Thirdly, a drug that is highly bound to albumin, and thus has a low unbound fraction ($F_{unbound}$), tends to be less available for diffusion into tissues. Lastly, the B:P is determined by the affinity for the red blood cells. A B:P < 1 means that the compound barely gets into the erythrocytes, which potentially makes more drug available for tissue uptake [19].

In addition to physicochemical properties, lysosomal sequestration, EGFR abundance and hallmarks of NSCLC tumors may play a role in predicting the tumor-to-lung contrast. The hallmarks of interest are namely tumor vascularization, and the impact of an acidic and/or immune deprived microenvironement. Furthermore, because of differences in basicity, lysosomal sequestration is expected to play a role in the differences in tracer uptake. Lysosomes are acidic membrane-bound organelles inside of tissue, which are capable of digesting biomolecules [20]. This traps the tracer in the lysosome, and affects the tissue uptake. Additionally, the prospect is that differences in affinity for EGFR (kd), and thus a difference in attraction to (target) tissue, in combination with a variation in EGFR abundance changes the tissue uptake [21,22]. Especially between lung tumor and lung tissue. Lastly, hallmarks of NSCLC like erratic tumor neovascularization, altered perfusion, and lowered immunogenic activity could possibly be of importance. These compound, tissue- and disease-specific properties may influence the whole-body distribution resulting in different tumor-to-lung contrasts of the three compounds.

Table 1: Compound specific physiochemical properties of erlotinib, afatinib and osimertinib.

	Erlotinib	**Afatinib**	**Osimertinib**
Log P[1]	3.3	3.6	3.2
pKa[1]	5.5	8.2	9.0
Acid or base	Weak base	Strong base	Strong base
B:P ratio[2]	0.95	1.27	0.79
Kd EGFR (nM)[3]	2164	2	155
$F_{unbound}$[1]	0.088	0.095	0.017

References: [1] Colclough (2021), [2] van de Stadt (2021), [3] joly-Tonetti (2021)

To gain a mechanistic understanding of processes underlying the observations a physiologically-based mathematical equation can be designed. Physiological modeling aims to integrate the knowledge of physiological processes and extent them with the compound-specific attributes in order to predict complex biological properties [23]. It is known that the extent of tissue distribution is defined by the tissue partition coefficient (e.g. the TBR), which depends on compound characteristics and the tissue composition [23,24]. With the equation, distribution to the tissues and thus tumor-to-lung contrast as a way to assess image quality can be predicted. Although physiologically-based models are frequently used in pharmacologic research, not much research has been done using these in relationship to PET tracers. An advantage of such mechanistic models is their predictive potential [23].

In earlier research the effect of the physiochemical properties and lysosomal sequestration on the role off TKI uptake was already evaluated. However, erlotinib predictions were not accurate yet and further extensions were needed [25]. For this research project we wish to add target specific binding to EGFR and hallmarks of NSCLC tumors. We hypothesized that by including the physicochemical properties, lysosomal sequestration, EGFR specific target-binding and/or hallmarks of NSCLC tumors in the models the tumor-to-lung contrast can be predicted. We developed two physiologically-based mechanistic models reflecting the essential features of tissue distribution of EGFR-TKIs. To assess the the difference in image quality, the aim of the researchproject is to predict the image quality by predicting the right tumor-to-lung contrast and secondly, predict the whole-body distribution. When fully validated, these mechanistic equations can be applied to predict tumor drug uptake in a wide array of diseases with structurally diverse compounds. As a result it could be used to steer drug development to compounds with high tumor-to-lung contrast. This would indicate a relatively higher uptake, and thus effect, in the tumor and less in the surrounding tissue.

Methods

R software within the Rstudio interface (version 4.0.3; R Foundation for Statistical Computing, Vienna, Austria) was used for simulations and graphical visualization of the predictions and PET observations were done using the package ggplot2 (Wickham, 2009) [26,27]. PET-TBR data was used to validate the equations [17].

Scan data

The reference data orginates from the study of *van de Stadt et al*.[17]. All PET scans were performed in advanced stage, EGFR mutated NSCLC patients. No patients were treated with the treatment analog of the PET tracer prior to scanning (e.g., a patient undergoing ^{11}C-erlotinib scanning was treatment-naïve for erlotinib). The PET-data used in this research is derived from static, 40-60 min post tracer dose whole-body PET/CT scans. All regions of interest were delineated by the same experienced researcher in a standardized manner using in-house developed software. For all tracers spleen, kidney, tumor, lung (contralateral from tumor site) and vertebra was included. For afatinib and osimertinib brain was additionally delineated but erlotinib scans did not include brain tissue in field of view. The full scan protocol and evaluation of the biodistribution is currently under submission [17].

Modelling strategy

Base models selection

The biodistribution of basic lipophilic drugs, like the three researched EGFR-TKIs, has been described extensively by well-established methods to predict the tissue partitioning [24,28]. Rodgers *et al* models provide the most accurate tissue distribution predictions [24,28,29]. The choice of model is dependent on compound properties, most importantly basicity. Relevant physicochemical properties used in modelling of the 3 EGFR TKIs erlotinib, afatinib and osimertinib can be found in **Table 1**. Since erlotinib is a weak base and osimertinib and afatinib are strong basic drugs, two base models are used. Model 1 is applicable for predicting tissue uptake of weak basic drugs and was used for erlotinib [28]. Model 2 can be used for afatinib and osimertinib predictions since this model applies for strong basic compounds [24].

The following assumptions were made in all models as validated by Rogers *et al*: drug transport only occurs passively; conditions are non-saturating; the drug is at steady state and well-stirred in all tissues of interest; metabolism and drug clearance are negligible at the time of scanning (at <0.05 of the biological half-life); the tissue PET scans did not contain a significant number of blood vessels (in the models only the concentration outside of the blood perfusing the tissue was calculated) [24,28].

Base models - Physicochemical drug distribution

In the physicochemical model, tissue-to-plasma ratio's (Kpu) are predicted based on distribution to albumin (ALB), neutral lipids and phospholipids (NL/NP), acidic phospholipids (AP-) and to cellular spaces such as the extra- and intracellular water (EW and IW). The described physicochemical base models predict Kpu at steady state by inclusion of drug-specific physicochemical properties and tissue composition (**Table 1&2**). If available, drug-specific properties were adapted from the PET imaging data, such as the blood-to-plasma ratio (**Table 1**). Physicochemical properties including pKa values were retrieved from the same *in vitro* research publication to prevent insecurities and enable comparison of the outcomes and can be found in **Table 1** [10].

Base model 1, the model reflecting weak bases, predicts the Kpu by calculation of the pH driven distribution to cellular components (Eq. 1). Tissue-specific fractional tissue volumes of cellular components, including intracellular water, extracellular water, neutral lipids and neutral phospholipids are reflected by respectively F_{iw}, F_{ew}, F_{nl}, and F_{np}. By use of the pH values of the cellular components intracellular water, neutral lipids and neutral phospholipids pH_{iw}, pH_{nl}, pH_{np} relative to the pH of plasma (pH_p), the fraction unprotonated drug available for diffusion to these cellular parts is predicted. pH values of the cellular components are shown in **Table 2.** The

octanol/water partition coefficient (P) is included for binding affinity of the unprotonated drug to neutral lipids and phospholipids in the cell membrane. Since a weak base such as erlotinib is highly (99%) unprotonated in plasma, albumin binding in the extracellular water is a predominant process of tissue distribution. The albumin binding was predicted based on the multiplication of an estimated association constant (Ka) for albumin with the tissue specific albumin concentration [28]. The formula for calculating the Ka is depicted in equation 2. A schematic overview of model 1 is depicted in **Figure 2B.**

(Eq. 1) $$\boldsymbol{Kpu}_{\text{R1}} = \left[\left(\frac{1+10^{pKa-pHiw}}{1+10^{pKa-pHp}} * \boldsymbol{fiw}\right) + \boldsymbol{few} + \left(\frac{P*Fnl,t+(0.3P+0.7)*Fnp,t}{1+10^{pKa-pHp}}\right) + (\boldsymbol{Ka,albumin} * [\boldsymbol{ALBUMIN}],\boldsymbol{tissue})\right]$$

(Eq. 2) $$\boldsymbol{Ka}_{\text{albumin}} = \left[\left(\frac{1}{\boldsymbol{Funbound}} - 1 - \left(\frac{P*Fnl,p+(0.3P+0.7)*Fnp,p}{1+10^{pKa-pHp}}\right)\right) * \left(\frac{1}{[ALBUMIN]p}\right)\right]$$

In model 2, the model reflecting strong bases, the pTBR contains the same elements for the distribution to neutral (phospho)lipids, intracellular and extracellular water (Eq. 3). In contrast to weak bases, afatinib and osimertinib are strong basic drugs (pKa >7) and are mostly protonated (respectively 98% and 86%) at physiological pH levels [10]. This protonation leads to binding to acidic phospholipids (AP-). Distribution to acidic phospholipids was predicted using association constant Ka [24].The Ka for AP- was calculated by subtracting the affinity for the cellular components of the partitioning to the red blood cells (Eq. 4). A schematic overview of model 2 is depicted in **Figure 2B.**

(Eq. 3) $$\boldsymbol{Kpu}_{\text{R2}} = \left[\left(\frac{1+10^{pKa-pHiw}}{1+10^{pKa-pHp}} * \boldsymbol{fiw}\right) + \boldsymbol{few} + \left(\frac{Ka*[AP-]*10^{pKa-pHiw}}{1+10^{pKa-pHp}}\right) + \left(\frac{P*Fnl,t+(0.3P+0.7)*Fnp,t}{1+10^{pKa-pHp}}\right)\right]$$

(Eq. 4) $$\boldsymbol{Ka}_{\text{AP}} = \boldsymbol{Kpu,bc} - \left(\frac{1+10^{pKa-pHbc}}{1+10^{pKa-pHp}} * \boldsymbol{fiw,b}\right) - \left(\frac{P*Fnl,b+(0.3P+0.7)*Fnp,b}{1+10^{pKa-pHp}}\right) * \left(\frac{1+10^{pKa-pHp}}{[AP-]*10^{pKa-pHbc}}\right)$$

Extension - EGFR target binding

Only non-specific binding is described by the physicochemical base models. Intracellularly, TKIs will bind with high affinity to EGFR [7,30]. Differences in affinity of EGFR-TKIs for their target may influence tissue binding and is therefore an essential feature for tissue distribution of TKIs. By adding EGFR binding to base models 1 and 2, target binding was included in the mechanistic model . Tissue-specific EGFR concentrations ([EGFR]) and drug-specific dissociation constants (Kd) for wild type EGFR are shown in **Table 1**. For two tissues of interest, bone and brain that lacked relevant literature data, we assumed EGFR was not present.

The contribution from EGFR has been taken into account following Rodgers' way of adding the parameters. Only what is present in the intracellular water (IW) can bind to EGFR. Assumed was that B and BH^+ equally bind to EGFR. So the total unbound concentration in the intracellular water ($\boldsymbol{C,iw}$) can bind to EGFR, according to Rodgers that equals to:

$$(1 + 10^{pKa-pHiw}) * \boldsymbol{fiw}$$

The amount that actually binds to EGFR is dependent on the concentration ($[\mathbf{EGFR}]$) and the affinity for EGFR ($\boldsymbol{Ka} = \left(\frac{1}{Kd}\right)$). Addition to the $\boldsymbol{C,iw}$ results in the concentration bound to EGFR ($\boldsymbol{C}_{\text{EGFR}}$):

$$\boldsymbol{C}_{\text{EGFR}} = \left(\frac{[EGFR]}{Kd}\right) * (1 + 10^{pKa-pHiw}) * \boldsymbol{fiw}$$

The tumor to plasma water partition coefficient ($\mathbf{Kpu}$) is calculated as follows:

$$\boldsymbol{Kpu} = \left(\frac{\boldsymbol{C,tissue}}{\boldsymbol{C,p}}\right)$$

The concentration in plasma $\boldsymbol{C,p}$ is defined as:

$$\mathbf{1} + \mathbf{10}^{\boldsymbol{pKa-pHp}}$$

Substituting $\boldsymbol{C}_{\mathbf{EGFR}}$ and $\boldsymbol{C,p}$ into the equation for the $\boldsymbol{Kpu}$ results in the contribution of the binding to EGFR, to the total $\boldsymbol{Kpu}$ (Eq. 5).

(Eq. 5) $$\boldsymbol{Kpu}_{\mathbf{EGFR}} = \frac{\left(\frac{[\boldsymbol{EGFR}]}{\boldsymbol{Kd}}\right)*(\mathbf{1}+\mathbf{10}^{\boldsymbol{pKa-pHiw}})*\boldsymbol{fiw}}{\mathbf{1}+\mathbf{10}^{\boldsymbol{pKa-pHp}}} = \frac{\left(\frac{[\boldsymbol{EGFR}]}{\boldsymbol{Kd}}\right)*(\mathbf{1}+\mathbf{10}^{\boldsymbol{pKa-pHiw}})}{\mathbf{1}+\mathbf{10}^{\boldsymbol{pKa-pHp}}} * \boldsymbol{fiw}$$

Extension - Lysosomal sequestration

Due to the protonated status in an environment with physiological pH, the lysosomal trapping was added to the physicochemical base model for strong bases (model 2) only by equation 4 [31,32]. To estimate the binding the lysosome is included in two different ways. According to *Assmus et al.* the same composition is assumed for the lysosomal membrane as for the outer membrane of the cell. Since immune cells, mostly consist of a higher lysosomal volume and a lower lysosomal pH than normal tissue cells, tissue specific cell types were included to predict the TBR (Eq. 6) [31]. According to *Schmitt et al*. binding to the membrane should not be included, because the exact composition is unknown. Thereby, it was stated that inclusion potentiely leads to an overprediction. Because of this reason only pH driven partiotioning was included [32]. Assmus' and Schmitts method were both included in the analyses to determine the correct one.

(Eq. 6) $$\boldsymbol{Kpu}_{\mathbf{lys\ 1}} = \left[\left(\frac{\mathbf{1}+\mathbf{10}^{\boldsymbol{pKa-pHlys}}}{\mathbf{1}+\mathbf{10}^{\boldsymbol{pKa-pHiw}}} * \boldsymbol{fiw}\right) + \left(\frac{\boldsymbol{Ka}*[\boldsymbol{AP-}]*\mathbf{10}^{\boldsymbol{pKa-pHlys}}}{\mathbf{1}+\mathbf{10}^{\boldsymbol{pKa-pHiw}}}\right) + \left(\frac{\boldsymbol{P}*\boldsymbol{Fnl}+(\mathbf{0.3}\boldsymbol{P}+\mathbf{0.7})*\boldsymbol{Fnp}}{\mathbf{1}+\mathbf{10}^{\boldsymbol{pKa-pHp}}}\right)\right]$$

(Eq. 7) ` $$\boldsymbol{Kpu}_{\mathbf{lys\ 2}} = \left(\frac{\mathbf{1}+\mathbf{10}^{\boldsymbol{pKa-pHlys}}}{\mathbf{1}+\mathbf{10}^{\boldsymbol{pKa-pHp}}} * \boldsymbol{flys}\right)$$

The models with the combination of physicochemical properties, the extension of EGFR and lysosomal sequestration, is illustrated in **Figure 2**. **Figure 2A** shows the place of the models on a systemic level, with **Figure 2B** on a cellular level.

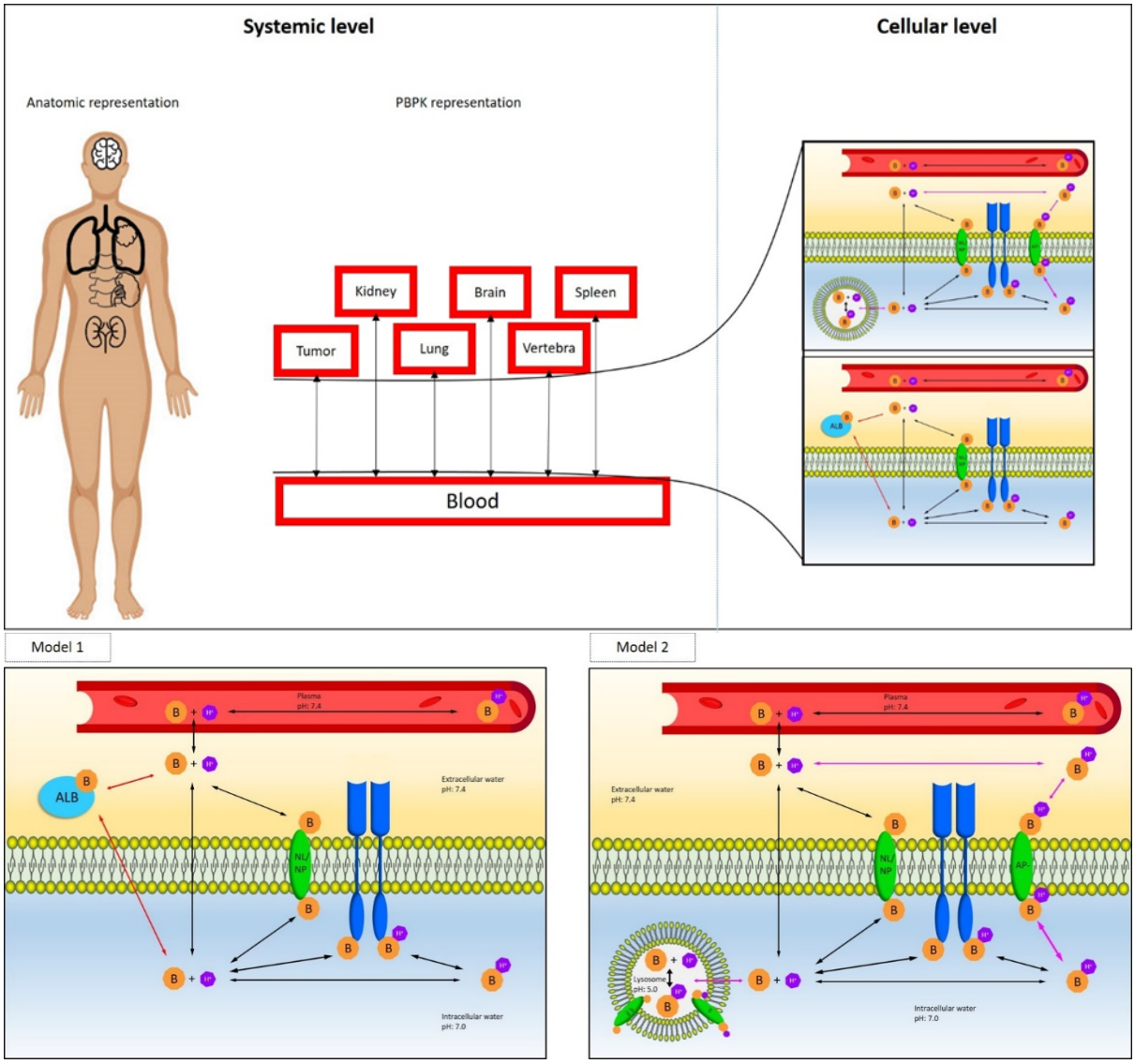

Figure 2. a) *Systemic (upper) and cellular levels (lower) of the models. Black arrows indicate transport of the drug between whole blood and tissues.* ***b)*** *Schematic overview of the mechanistic models for weak basic EGFR-TKIs (Model 1) and strong basic EGFR-TKIs (Model 2). The plasma compartment is depicted in red, extracellular space in yellow and intracellular space in blue. Orange hexagons "B" (base) depict the drug, purple hexagons depict H+ atoms. When depicted together, bases are protonated. When depicted separately, the base is unprotonated. Blue receptors depict epidermal growth factor receptor (EGFR), green ovals over the cell membranes are neutral (phospho)lipids (NL/NP) and acidic phospholipids (AP-). Light blue ALB is a representation of albumin. Black arrows depict processes that are included in both models, red/purple arrows depict processes specific for each model. pH values for each compartment are given. Equations for model 1 and 2 below and the model structure are further explained in the supplement A-II and III.* ***B****= basic unprotonated drug,* ***BH+****= protonated drug, AP-=acidic phospholipids,* ***NL*** *=neutral lipids* ***PL****=phospholipids,* ***ALB****= albumin,* ***EGFR****=epidermal growth factor receptor*

Inclusion hallmarks of NSCLC

Three of the hallmarks of NSCLC tumors are a potential immune-suppressive micro-environment, erratic (and potential inadequate) neovascularization and perfusion caused by changes in the micro-environment [34-36]. We hypothesized that either of these hallmarks could predict a decreased cellular concentration of the TKIs, even at a high affinity and higher expression of EGFR in the tumor.

The impact of the lysosomal volume of different cell types on tissue uptake in tumor compared to normal lung was researched. Lung tissue uptake was simulated with the equation of *Assmus et al.* by use of a physiological composition including the different immune cells: 4.1% alveolar macrophages, 8.3% type II cells and 87.6% residual cells (**Table 2**) [31]. Of these three the residual cells are the least immunogenic cells. To reflect an

immune-suppressive micro-environment, tumor tissue uptake with input parameters concerning only (100%) residual lung cells was applied in the equation of *Assmus et al.*

As a final a final hallmark, we hypothesized that the number of vessels drives drug penetration. The vascular coefficient was calculated by dividing the microvessel density (MVD) of normal lung tissue (4 samples), obtained from the Human Protein Atlas by the MVD of 8 samples of adenocarcinoma NSCLC patients. MVD was calculated per surface area of CD31+ vessels and tissues. A full description of this analysis can be found in **Appendix I**. The MVD tumor vs lung ratio (Fvasc) was calculated and multiplied with the Kpus. Since tumor uptake of ^{11}C-erlotinib and ^{18}F-afatinib has previously been shown to be independent of tumor perfusion, we assumed that all three EGFR TKIs were perfusion independent [11,15].

After inclusion of all drug specific, tissue properties and disease properties, the full models is derived. The full models are depicted in Equation 8 and 9.

(Eq. 8) $$\boldsymbol{Kpu_{\text{Full 1}} = F_{vasc/perf} * \left(Kpu_{R1/R2} + Kpu_{EGFR} + Kpu_{lys1/2}\right)}$$

(Eq. 9) $$\boldsymbol{Kpu_{\text{Full 2}} = F_{vasc/perf} * \left(Kpu_{R1/R2} + Kpu_{EGFR}\right)}$$

Simulation tumor-to-lung and tissue distribution

The PET-data was calculated in tissue-to-blood ratios (TBR). As a final step, to compare the predicted values to the observed PET-values the tissue-to-plasma ratios were recalculated to tissue-to-blood ratios (pTBR) with the affinity to red blood cells (KpuBc) (Eq. 10). The KpuBc was calculated by the hematocrit, Funbound and bp, illustrated in equation 11.

(Eq. 10) $$\boldsymbol{pTBR = \frac{Kpu_{Full\ 1/2}}{KpuBc}}$$

(Eq. 11) $$\boldsymbol{Kpu, bc = \left(\frac{H - 1 + (B:P)}{Funbound * H}\right)}$$

For all EGFR-TKIs, the tumor-to-lung contrast was estimated by dividing the uptake in tumor by the uptake in lung (*contrast = pTBR tumor/pTBR lung*). This contrast was subsequently validated with the PET imaging data. Furthermore, tissue distribution was assessed by predicting the TBR of the lung, tumor, spleen, kidney, brain and bone and compared to PET imaging tissue uptake data.

Statistics

The accuracy of mechanistic equation predicted tumor-to-lung contrast and the TBR was assessed by determination of the percentage of tissues falling within 3-fold of observed data, as is done in the referenced research by Rodger *et al*. [24,28]. This was researched by calculating prediction errors (PE) and mean prediction error of the model and of subsequent sensitivity analyses. The strength of correlation between the predicted and the PET image observed TBR was assessed by the R squared and with a two-sample t-test significance of the correlation was determined.

$$PE = \left(\frac{PRED - OBS}{mean(PRED + OBS)}\right) * 100\% \qquad R = 1 - \frac{\sum(\text{yi} - \hat{\text{y}}^{\text{i}})2}{\sum(\text{yi} - \overline{\text{y}})2}$$

Sensitivity analyses were performed by researching the impact of extension with EGFR binding, use of a different lysosomal extension models on tissue-to-blood ratios and the effect of tumor immune deprivation on all tissues

of interest. The effect of the aberrant tumor vasculature was determined by comparing the results after inclusion of a vascular versus the (unaltered) perfusion coefficient. When in sensitivity analyses the removal of the extension of the base models showed a significant decrease in predictivity the PE (mean > 10%) of the tumor-to-lung contrast of all three models, the component was retained in the final models.

*Table **2** Tissue and compound specific input parameters. Tissue specific parameters were adapted from Table 1 Rodgers et al. 2005, Table 1 Rodgers et al. 2006 and Table 1 Schmitt et al. 2021, EGFR concentrations from Table 3 Glassman et al. 2016, lung specific parameters from Table 1 Assmuss et al. 2017.*

Tissues specific input parameters								
	F_{nl}	**F_{np}**	**F_{ew}**	**F_{iw}**	**F_{lys}[b]**	**Tissue concentration of AP^- (mg/g)[b]**	**Albumin tissue to plasma ratio[c]**	**EGFR (nM)**
Blood cells	$1.7*10^{-3}$	0.0029	n.a.	0.60	n.a.	0.50	n.a.	n.a.
Bone	0.017	0.0017	0.1	0.35	n.d.	0.67	0.10	n.a.
Brain	0.039	0.0015	0.16	0.61	0.014	0.40	0.048	n.a.
Kidney	0.039[a]	0.012[a]	0.27	0.47	0.017	2.44[1]	0.13	177
Lung[c]	0.0088[a]	0.0030[a]	0.34	0.43	0.015	0.57[a]	0.21	31.1
Tumor					0.01			299
Spleen	0.021[a]	0.017[a]	0.21	0.53	0.053	3.18	0.097	54.6
Plasma[d]	n.a.	n.a.	n.a.	n.a.	n.a.	n.a.	n.a.	n.a.
Lung specific input parameters[2]								
	F_{nl}	**F_{np}**	**F_{ew}**	**F_{iw}**	**F_{lys}**	**pH lysosome**	**$F_{cell\ type}$**	
<u>Lung</u>	0.0088[a]	0.0030[a]	0.34	0.45				
- Alveolar macrophages					0.078	4.75	0.041	
- Type II cells					0.03	5.1	0.083	
- Residual cells					0.01	5.1	0.88	

[a]Translation factor from rats to human [24,28].[b] Input parameter only used in model 1. [c]Input parameter only used in model 2 Lung pH,bc: 7.22; pHp 7.4; pHiw 7.0; pHlys: 5.3. [d]Hematocrit (H): 0.45; [5]Blood to plasma concentration ratio. [e]Unprotonated fraction [10]. F_{iw}, F_{ew}, F_{nl}, and F_{np} reflect tissue-specific fractional tissue volumes of the cellular components intracellular water, extracellular water, neutral lipids and neutral phospholipids. Flys, pHlys and Fcell reflect lysosomal volume fraction, lysosomal pH and the fraction of various cell types in tissue. Fvasc : 0.36 **Appendix I**, and Fperf: 1 reflect the vascular and perfusion coefficient in the tumor compared to the surrounding lung tissue.

Results

Model building

Our main goal was to predict the right tumor-to-lung contrast. To acquire the most accurate model, sensitivity analyses that excluded different parameters of the full models was done (table 3). The one with the most accurate contrast for all three TKIs was renamed to the "final model", Equation 12 and 13. The final models consisted of physicochemical drug distribution, lysosomal sequestration (for the strong bases; as included by *Assmus et al*.), tumor immune deprivation and unaltered tumor perfusion and EGFR target binding, but excluded vascularization.

(Eq. 12) $$\boldsymbol{Kpu_{\text{Full 1}}} = \frac{\boldsymbol{F_{vasc/perf}} * \left(\boldsymbol{Kpu_{R1/R2}} + \boldsymbol{Kpu_{EGFR}} + \boldsymbol{Kpu_{lys1/2}}\right)}{\boldsymbol{Kpu,BC}}$$

(Eq. 13) $$\boldsymbol{Kpu_{\text{Full 2}}} = \frac{\boldsymbol{F_{vasc/perf}} * \left(\boldsymbol{Kpu_{R1/R2}} + \boldsymbol{Kpu_{EGFR}}\right)}{\boldsymbol{Kpu,BC}}$$

Model building - Lysosome

The influence of including only a pH driven approach for lysosomal sequestration (excluding lysosomal membrane binding distribution) (eq 6) in the model was simulated. The correct tumor-to-lung contrast was not simulated by using this simplified approach for lysosomal sequestration, indicated by the increase in PE for both afatinib and osimertinib (Afatinib PE 44% to 92%, Osimertinib: -7.5% to +26% see **Table 3**). Although the PE decreased for lung TBR in afatinib, tumor TBR remained relatively similar, leading to a worse outcome when tumor-to-lung contrast was simulated.

Model building - EGFR

The influence of EGFR on the mechanistic model was researched by simulation of the model without EGFR binding. This model without EGFR was not able to capture the right tumor-to-lung contrast for mainly afatinib (PE 43% to -64%). Contrary to the observed contrast, without EGFR target binding a higher uptake in lung than in tumor was predicted for afatinib. (**Table 3**) The model including EGFR was able to capture the image quality by predicting the right predictive values in 67% of tissues for afatinib, 100% (osimertinib) and 16% (erlotinib), within 3-fold of the observed values (**Table 3**).

Model building – Immune depriviation

Immune deprivation in the tumor tissue may lead to less macrophages and type II cells in the tumor core, influencing distribution to the tumor. In the final model, this is corrected by adding the fraction F_{cell} (**Table 2**) to healthy lung tissue, but not to tumor tissue, simulating immune deprivation in tumor tissue. To analyze whether this difference in immune cell presence plays a role in determining drug distribution, we added the same fraction immune cells to the tumor tissue as well. This model showed a worse outcome when compared to the mechanistic model as described above (**Table 3**), leading to a decrease in accuracy predicting afatinib tumor tissue (PE 108% to 115%**)**and a decrease in accuracy predicting tumor-to-lung contrast for both afatinib (PE 44% to 53%) and osimertinib (PE -7.5% to 23%, **Table 3**). Since erlotinib is a weak base, immune deprivation was not simulated.

***Table 3**: Sensitivity analyses of extensions of the final mechanistic PBPK-model. The final model included physicochemical drug distribution, lysosomal sequestration, tumor immune deprivation and unaltered tumor perfusion and EGFR target binding, but excludes vascularization. 1) Final model without membrane lysosome 2) final model without EGFR binding 3) final model without tumor immune deprivation & 4) final model with tumor vascularization. The predicted TBR, observed PET TBR and the predicted vs observed Tumor-to-lung ratio are shown. TL-ratio: Tumor-to-lung ratio.*

			Erlotinib			Afatinib			Osimertinib		
			Lung	Tumor	TL-ratio	Lung	Tumor	TL-ratio	Lung	Tumor	TL-ratio
Final	Mechanistic model	Predicted	0.30	0.30	1.02	5.47	12.13	2.22	4.60	3.42	0.74
		Observed	0.51	1.42	2.78	2.54	3.60	1.42	7.01	5.60	0.80
		PE (%)	**-52.64**	**-129.61**	**-92.79**	**73.27**	**108.43**	**43.88**	**-41.42**	**-48.50**	**-7.45**
Sensitivity analysis	1) model – membrane lysosome	Predicted				2.78	10.66	3.84	1.88	1.94	1.03
		PE (%)				**9.12**	**99.04**	**92.00**	**-115.40**	**-97.24**	**26.23**
	2) model – EGFR	Predicted	0.30	0.30	1.00	4.55	3.33	0.72	4.59	3.35	0.73
		PE (%)	**-52.84**	**-131.76**	**-94.19**	**56.91**	**-7.93**	**-64.12**	**-41.56**	**-50.27**	**-9.19**
	3) model – tumor immune deprivation	Predicted				5.47	13.35	2.44	4.60	4.66	1.01
		PE (%)				**73.27**	**115.07**	**52.96**	**-41.42**	**-18.38**	**23.49**
	4) model – addition vascularization	Predicted	0.30	0.11	0.37	5.47	4.37	0.80	4.60	1.23	0.27
		PE (%)	**-52.64**	**-171.44**	**-153.41**	**73.27**	**19.21**	**-56.03**	**-41.42**	**-128.01**	**-99.82**

Model building – Perfusion/Vascularization

Using the mechanistic model, we hypothesized that not just perfusion but also vascularization of the tumor determines tumor drug penetration. Histological analysis of the healthy lung tissue samples and adenocarcinoma samples yielded a vasculature coefficient of 0.36, indicating that tumor tissue shows approximately 2.8 times less vessels per mm2 tissue than lung tissue (Appendix Figure 1). We assumed that all three EGFR TKIs were perfusion independent (15, 20). The influence of the variability in vascularization between tumor and non-tumorous long tissue was tested by including this vasculature reflection coefficient. The prediction of lung uptake decreased by including this parameter for all TKI, compared to the final model, presuming unaltered tumor perfusion (**Table 3,** PE -93 to -153%, 44% to -56% and -7.5 to -99% for erlotinib, afatinib and osimertinib respectively). Therefore, only the perfusion coefficient and not the vasculature coefficient was retained in the final models.

Model verification

The tumor-to-lung contrast was predicted using the final model to visualize differences in image quality observed in PET imaging, as shown in **Figure 3A**. The predicted TBR are shown in **Figure 3B**. Both observed and predicted TBR values showed high uptake of osimertinib and afatinib in lung and tumor tissue (TBR >1) and high blood concentrations compared to tissue concentrations for erlotinib (TBR< 1, **Figure 3**). Furthermore, tumor-to-lung contrast for all EGFR-TKIs was well predicted, i.e. a contrast >1 for afatinib and erlotinib and a contrast <1 for osimertinib **(Table 4).**

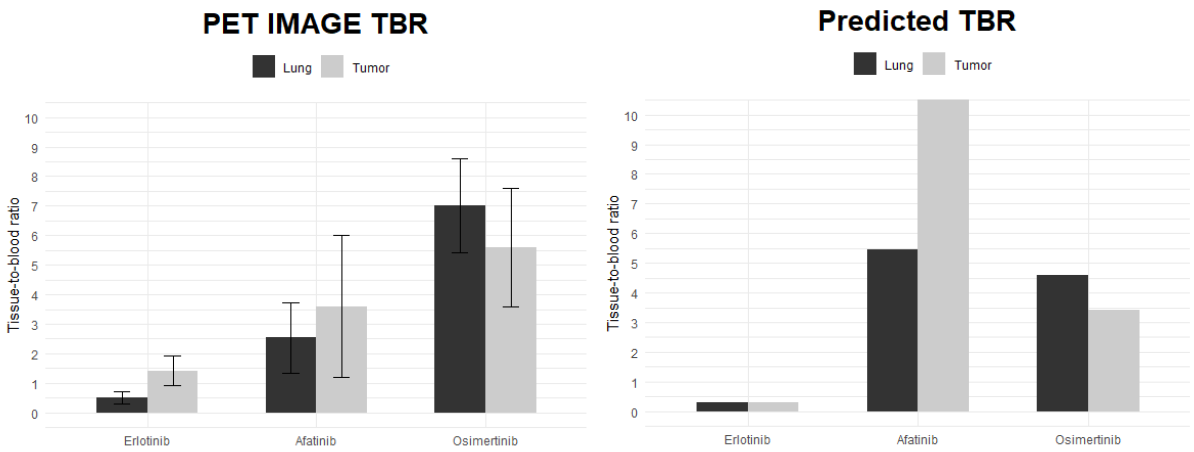

Figure 3: *The association between PET image derived TBR and model predicted TBR.* ***A)*** *PET image derived TBR (left) versus B) model predicted TBR of lung and tumor (right). For patient data, standard deviations are given.*

Table 4 describes the contribution of different components of the mechanistic model. Erlotinib binds extensively to albumin in tissue, whereas osimertinib and afatinib predominantly bind to AP- in the cellular membranes and are sequestered in the lysosome. Substantial decrease of lysosomal sequestration was predicted for both strong basic EGFR-TKIs in the less lysosome-rich tumor in comparison with lung tissue. Tumor EGFR binding of afatinib was predicted to be extensive for and comprised 72.58% of all tissue binding, whereas for erlotinib and osimertinib the model showed that only a minor fraction of the tissue fraction bound to EGFR (1.97 and 1.88% respectively).

The whole-body distribution of the three EGFR-TKIs was described by the mechanistic model. The predicted TBR values compared to the measured TBR (obtained during PET imaging) are shown in Figure 4 and Appendix Table 1. The model is able to predict the overall body distribution of the TKIs, with extensive distribution to most tissues for osimertinib and afatinib and limited tissue penetration for erlotinib. The observed and predicted TBR values of osimertinib and afatinib in most tissues were >1 and for <1 (Appendix table 1). The TBR predicted by the mechanistic model correlated strongly with the PET imaging data (R^2: 0.814 with $p < 0.0001$; $\alpha = 0.01$) with a mean PE of -2.91% (CI95% of the data: -114.6 to 108.8, **Figure 4**). For afatinib, 67% of tissues was predicted within a factor of 3 of the observed value. The data point falling outside this range represented brain uptake of afatinib, and was predicted to be 187.1% times higher than observed and tumor predictions, above the 3-fold limit of the observed mean value (Appendix Table 1). However, for osimertinib, 100% of tissues were predicted to be within 3-fold of the observed tissue uptake of PET imaging. For erlotinib, the model predicted the TBR compared to the observed ratio less accurately: only 16% of TBR were predicted within 3-fold of the observed values. The lung was predicted accurately with a PE of -52.6%. However, the predicted TBR of spleen, kidney, bone and tumor were underestimated (Appendix Table 1).

Table 4: contribution of the different components in the final mechanistic models to the predicted TBR in the lung and the tumor. NL/NP neutral (phospho)lipids; AP- acidic phospholipids; IW intracellular water; EW extracellular water.

	Erlotinib	**Afatinib**	**Osimertinib**
Lung			
IW	14.54%	1.08%	0.72%
EW	0.36%	0.36%	0.23%
NL/NP	1.12%	0.01%	0.00%
Albumin	73.01%	n.a.	n.a.
AP-	n.a.	32.63%	39.74%
EGFR binding	0.21%	16.73%	0.14%
Lysosomal trapping	n.a.	49.19%	59.16%
Tumor			
IW	14.28%	0.49%	14.28%
EW	10.93%	0.16%	0.31%
NL/NP	1.10%	0.00%	0.00%
Albumin	71.72%	n.a.	n.a.
AP-	n.a.	14.72 %	53.55 %
EGFR binding	1.97%	72.58 %	1.88%
Lysosomal trapping	n.a.	12.05%	43.30%

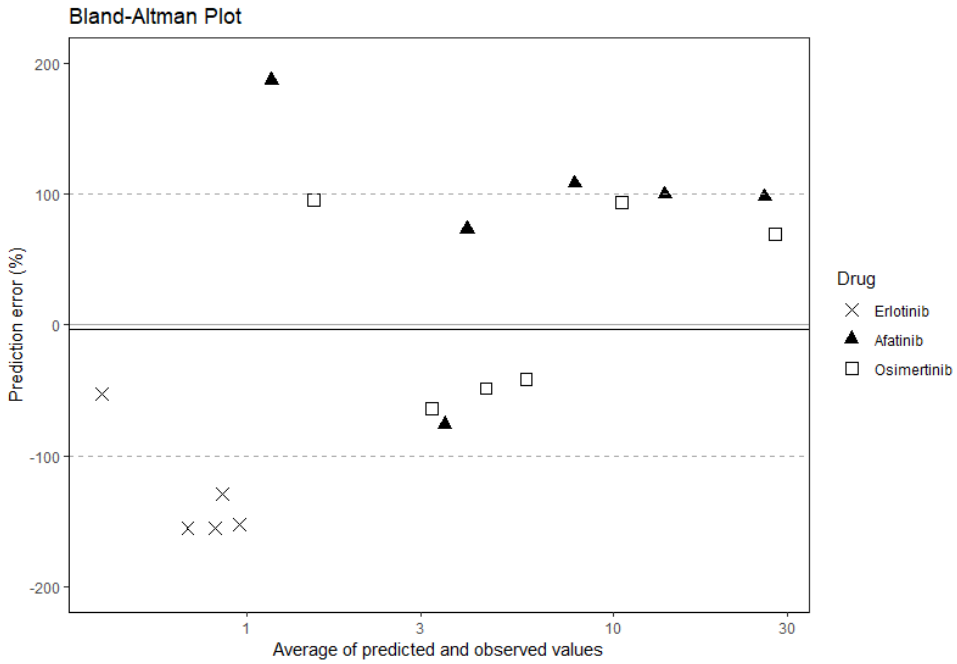

Figure 4 : Bland-Altman plot showing accuracy of the model to predict tissue uptake. The solid black line represents the mean, the dashed lines a factor 3 of both sides of zero. Percentage of predictions falling within 3-fold: erlotinib 20%,afatinib 67%, osimertinib 100%

Discussion

The mechanistic equations in this study were developed to capture essential features of tissue distribution by extending previously published physicochemical base models with EGFR binding, lysosomal sequestration and tumor immune deprivation at unrestricted tumor perfusion [9,14,37]. The developed models were able to capture the right tumor-to-lung contrast for all EGFR-TKIs and therefore was able to predict image quality. Furthermore, the models captured the right whole-body distribution with a high tissue distribution for osimertinib, to a lesser extent for afatinib and an underperdiction with low tissue distribution and high whole blood concentrations for erlotinib.

^{11}C-erlotinib reached relatively high concentrations in the blood compared to tissues (TBR<1), compared to ^{18}F-afatinib and ^{11}C-osimertinib. This relates to a small whole-body volume of drug distribution, which is similar to the volume of distribution estimated at therapeutic dose levels (erlotinib 232L, afatinib 2370L and osimertinib 918L) [38-40]. It is shown that the models based on physicochemical drug properties of the TKI's predicted these differences in distribution profiles. Furthermore, the negative tumor-to-lung contrast as seen by ^{11}C-osimertinib is also predicted by the models including these parameters.

For osimertinib, we hypothesized that a lower lysosomal volume in tumors, assuming an immune suppressive microenvironment, would lead to a decreased cellular concentration of osimertinib compared to lung tissue. Indeed, this resulted in a correctly predicted tumor-to-lung contrast for osimertinib. Since the decrease in lysosomal sequestration mainly impacts the tumor uptake (**Table 4**), we showed that the low tumor-to-lung contrast for osimertinib may be explained by immune deprivation and subsequent decrease in lysosomal volume in tumor tissue. The same phenomenon was observed for other TKIs like nintedanib where increased lysosomal number and lysosomal size decreases sensitivity towards these drugs [41]. This hypothesis is further strengthened by the sensitivity analysis where immune deprivation is excluded from the model. This models was less accurate in predicting uptake, indicating that immune cells play a significant role in tissue uptake.

For afatinib, the predicted decrease in lysosomal sequestration in tumor compared to lung was accompanied by a relative high percentage of EGFR binding (**Table 4**). For all three compounds, the tumor-to-lung contrast was predicted adequately after accounting for EGFR binding in the model. For afatinib, EGFR binding had the highest influence on tumor distribution in the mechanistical model due to its low dissociation constant (K_D) [37,42]. EGFR binding showed the highest contribution to the overall tissue uptake. As shown in the sensitivity analyses, when EGFR-binding is removed, tumor-to-lung contrast was highly underpredicted. However, tumor tracer uptake of erlotinib and osimertinib was underpredicted by the models and erlotinib fell outside of the 3-fold range. We hypothesize that variation in EGFR abundance and target affinity among patient-tumors relates results in high variability in tumor tracer uptake. Erlotinib and osimertinib EGFR binding may be underpredicted as affinity for wild type EGFR was applied. Previous research from our group provided the framework for EGFR binding in tissue by demonstrating the ability of PET/CT to distinguish between wild-type and mutated EGFR [13,14,15]. Therefore, future studies should include EGFR binding affinities for mutated and wild-type receptors, specifically for drugs with differences in affinity between wild type and mutation.

The distribution for drugs into tissues with high drug transporter abundancy, e.g. brain, kidney and spleen, was less accurate. For erlotinib, only lung (an organ unaffected by drug transporters) was predicted correctly. For erlotinib, the underpredictions of the other tissues of interest are likely explained by the effect influx transporters. Erlotinib is a substrate for the influx transporters OAT3 and OCT2 [21]. In rats the influence of the influx transporter OAT on tissue distribution of erlotinib was investigated in a ^{11}C-erlotinib PET imaging study. The OAT influx transporter was inhibited by rifampicin and decreasing erlotinib exposure was measured in the kidneys and liver, but the exposure in lung was unaffected [43] . The overprediction of the TBR for the brain of afatinib may be caused by drug efflux by MDR1 and the BCRP [10]. These drug efflux transporters are highly abundant in the blood-brain barrier (BBB). Similar to the observations of the PET study of *van de Stadt et al.*, a preclinical permeability study showed a low brain-to-blood ratio of 0.31 for afatinib [10]. In future studies both influx and efflux transport processes should be studies and research in how to optimally implement these processes is needed.

Another possible explanation for underprediction is that albumin binding may not be the only process of tissue distribution to be accounted for. Multiple lipophilic, basic drugs bind with a high affinity to the immune-activated protein alpha-1-acid glycoprotein (AAG) [44]. Prior studies show that in plasma of NSCLC patients AAG levels are increased, but little is known of AAG in the extracellular water of tissues during cancer. Potentially in lysosomal rich tissues such as lung, AAG levels may be higher compared to the immune-suppressive microenvironment of the tumor. As the role of AAG in plasma binding and drug transport of weak bases has been established, further research of the role of AAG for tissue distribution is needed [45].

Sensitivity analysis demonstrates the need for inclusion of the lysosomal membrane, since the correct tumor-to-lung contrast was not captured for all compounds when only a pH driven approach was included in the models . The high impact of lysosomal sequestration (**table 2**) after microdosed PET may be due to the unsaturated lysosomes. Fluoxetine, a basic lipophilic compound with comparable physicochemical properties (log P = 3.2, pKa = 9.8) to afatinib and osimertinib, shows that at prolonged exposure of therapeutic doses, lysosomal saturation curve occurs(43). When extrapolating the results to therapeutic PK, potential saturation of lysosomes needs to be accounted for. Furthermore, further research into nonlinear processes of drug binding and sequestration may improve the models predictions when comparing microdose and therapeutic dose PK [22, 46].

In the sensitivity analysis, vascularization driving drug penetration was studied as a hallmark of NSCLC tumors [35,36]. Our results show that vascularization does not drive drug penetration since the models performs worse when this component was added. Previous results have shown that tracer uptake is perfusion-independent. To our knowledge this is the first physiological modelling study that addresses these differences, as prior studies either did not account for variability in tumor vs. normal tissue or used a standardized value (e.g. 0.73 in colon cancer [47]. However, other hallmarks of cancer such as the collagen matrix and its effect on the penetration of drugs should be studied.

In this study the partitioning into the red blood cells (KpuBc) was used to recalculate the tissue-to-plasma ratios (Kpu) of the model to tissue-to-blood ratios (pTBR). However, in the literature there are multiple exampels models were the blood-plasma ratio (bp) was used to calculate the blood concentrations [48-50]. The blood-to-plasma ratio is defined as the blood concentration of the drug divided by the plasma concentration [48]. These findings question our choice to have used the KpuBc voor the translation of Kpu to TBR. Further exploration of these findings, and potential different outcomes, is needed.

Conclusion

Our mechanistic models consisting of a base models dependent on physicochemical properties of the relevant drug, EGFR binding, lysosomal sequestration and tumor immune deprivation and unaltered tumor perfusion was able to accurately predict tumor-to-lung contrast. We therefore conclude that our mechanistical models accurately predicts image quality for EGFR expressing NSCLC tumors, while further study of distribution for drugs into tissues with high drug transporter abundancy and the effect of EGFR mutation on drug penetration is needed.

Limitations

In this study, we have extended previously published physicochemical base models with EGFR binding and lysosomal sequestration. These base models were validated with *in vivo* data obtained at steady state therapeutic drug concentrations. The PET imaging data used in this study was obtained 1-2 hours after a single microdose [12,15,16]. Therefore, it should be noted that discrepancies between predicted and observed TBR may occur due to lower drug exposure and non-steady state. Furthermore, drug metabolism and elimination was not taken into account. The half-life of the three researched EGFR-TKIs was comparable and greatly exceeded the 1-2 hour scan period (erlotinib = 36 h; afatinib = 45 h; osimertinib = 49 h), making the assumption of absence of elimination reasonable [38-40]. Prior research of midazolam, a compound with similar metabolic profile to erlotinib, suggests that metabolism at microdose level is not different from metabolism at therapeutic

dose level [51]. However, when these models are applied for predicting the whole-body distribution and target uptake of new tracers with shorter half-lives, inclusion of metabolism and elimination might be needed.

Future perspective

If drug properties can be used to predict differences in image quality, it may be possible to predict tracers with an optimal image quality: drugs with large tumor/tissue contrast. Before applying these predictions in drug development, prospective validation of the predictive value of the models using new tracers are needed. Furthermore, to predict TBR in future studies more precisely, both active and passive influx and efflux transport needs to be included in the mechanistic models. Therefore, further *in vitro* research to binding affinities for transporters and transporter tissue concentrations is needed. The models also showed that the pH driven partitioning as a result of small differences in pH, play an important role in the tissue uptake. In the future the acidic tumor environement of NSCLC tumors of 6.7-7.1 should be added [52].

In order to study differences in tumor-to-lung contrast and whole-body distribution between microdose and therapeutic dose, the mechanistic models needs to be extended in a concentration-dependent matter. Injected dose of ^{11}C-erlotinib corresponded with 2.2 µg (±0.46) erlotinib. When compared to the regular therapeutic dose of 150 mg, this is a >10.000 fold difference [15]. With this difference in dosing, lysosomal sequestration, albumin, lipoprotein, AP^- and EGFR binding and EGFR-target binding will become saturated and by including these nonlinear processes, the influence of different doses on TBR can be assessed.

The impact of mutational status on tumor-to-lung contrast and whole-body distribution can be investigated by the use of affinity constants for EGFR wild type and mutated EGFR. First, the activating EGFR mutation needs to be identified in order to use the right affinity value, thereby increasing accuracy of the prediction of tumor uptake. **When fully validated such models, combined with optimized individual imaging-based uptake measurements, may predict individualized dosing regimens intended to optimize drug exposure at the site of disease, thereby improving drug-efficacy.**

References

[1] Sung H, Ferlay J, Siegel RL, Laversanne M, Soerjomataram I, Jemal A, et al. Global Cancer Statistics 2020: GLOBOCAN Estimates of Incidence and Mortality Worldwide for 36 Cancers in 185 Countries. CA Cancer J Clin. 2021 May;71(3):209-249. doi: 10.3322/caac.21660.

[2] Faehling M, Schwenk B, Kramberg S, Eckert R, Volckmar AL, Stenzinger A, et al. Oncogenic driver mutations, treatment, and EGFR-TKI resistance in a Caucasian population with non-small cell lung cancer: survival in clinical practice. Oncotarget. 2017;8(44):77897-914.

[3] Red Brewer M, Yun CH, Lai D, Lemmon MA, Eck MJ, Pao W. Mechanism for activation of mutated epidermal growth factor receptors in lung cancer. Proc Natl Acad Sci U S A. 2013;110(38):E3595-604.

[4] Yarden Y, Pines G. The ERBB network: at last, cancer therapy meets systems biology. Nat Rev Cancer. 2012 Jul 12;12(8):553-63. doi: 10.1038/nrc3309. PMID: 22785351.

[5] Lynch TJ, Bell DW, Sordella R, Gurubhagavatula S, Okimoto RA, Brannigan BW, et al. Activating mutations in the epidermal growth factor receptor underlying responsiveness of non-small-cell lung cancer to gefitinib. N Engl J Med. 2004 May 20;350(21):2129-39. doi: 10.1056/NEJMoa040938. Epub 2004 Apr 29. PMID: 15118073.

[6] Paez JG, Jänne PA, Lee JC, Tracy S, Greulich H, Gabriel S, et al. EGFR mutations in lung cancer: correlation with clinical response to gefitinib therapy. Science. 2004 Jun 4;304(5676):1497-500. doi: 10.1126/science.1099314. Epub 2004 Apr 29. PMID: 15118125.

[7] Eck MJ, Yun CH. Structural and mechanistic underpinnings of the differential drug sensitivity of EGFR mutations in non-small cell lung cancer. Biochim Biophys Acta. 2010;1804(3):559-66.

[8] Yun CH, Boggon TJ, Li Y, Woo MS, Greulich H, Meyerson M, et al. Structures of lung cancer-derived EGFR mutants and inhibitor complexes: mechanism of activation and insights into differential inhibitor sensitivity. Cancer Cell. 2007;11(3):217-27.

[9] Yi L, Fan J, Qian R, Luo P, Zhang J. Efficacy and safety of osimertinib in treating EGFR-mutated advanced NSCLC: A meta-analysis. Int J Cancer. 2019;145(1):284-94.

[10] Colclough N, Chen K, Johnstrom P, Strittmatter N, Yan Y, Wrigley GL, et al. Preclinical Comparison of the Blood-brain barrier Permeability of Osimertinib with Other EGFR TKIs. Clin Cancer Res. 2021;27(1):189-201.

[11] van de Stadt EA, Yaqub M, Lammertsma AA, Poot AJ, Schober PR, Schuit RC, et al. Quantification of [(18)F]afatinib using PET/CT in NSCLC patients: a feasibility study. EJNMMI Res. 2020;10(1):97.

[12] van de Stadt EA, Yaqub M, Lammertsma AA, Poot AJ, Schuit RC, Remmelzwaal S, et al. Identifying advanced stage NSCLC patients who benefit from afatinib therapy using (18)F-afatinib PET/CT imaging. Lung Cancer. 2021;155:156-62

[13] Bahce I, Smit EF, Lubberink M, van der Veldt AA, Yaqub M, Windhorst AD, et al. Development of [(11)C]erlotinib positron emission tomography for in vivo evaluation of EGF receptor mutational status. Clin Cancer Res. 2013;19(1):183-93.

[14] Bahce I, Yaqub M, Errami H, Schuit RC, Schober P, Thunnissen E, et al. Effects of erlotinib therapy on [(11)C]erlotinib uptake in EGFR mutated, advanced NSCLC. EJNMMI Res. 2016;6(1):10.

[15] Bahce I, Yaqub M, Smit EF, Lammertsma AA, van Dongen GA, Hendrikse NH. Personalizing NSCLC therapy by characterizing tumors using TKI-PET and immuno-PET. Lung Cancer. 2017;107:1-[16] Yaqub M, Bahce I, Voorhoeve C, Schuit RC, Windhorst AD, Hoekstra OS, et al. Quantitative and Simplified Analysis of 11C-Erlotinib Studies. J Nucl Med. 2016;57(6):861-6.

[17] van de Stadt EA. Relationship between biodistribution and tracer kinetics of 11C-erlotinib, 18F-afatinib and 11C-osimertinib and image quality evaluation using pharmacokinetic/pharmacodynamic analysis in advanced stage non-small cell lung cancer patients. Diagnostics. 2022 [In Submission]

[18] Rowland, Malcolm., Thomas N. Tozer, and Malcolm. Rowland. Clinical Pharmacokinetics and Pharmacodynamics : Concepts and Applications. 4th ed. Philadelphia: Wolters Kluwer Health/Lippincott William & Wilkins, 2011. Print.

[19] Mamada H, Iwamoto K, Nomura Y, Uesawa Y. Predicting blood-to-plasma concentration ratios of drugs from chemical structures and volumes of distribution in humans. Mol Divers. 2021 Aug;25(3):1261-1270. doi: 10.1007/s11030-021-10186-7.

[20] Hallifax D, Houston JB. Saturable uptake of lipophilic amine drugs into isolated hepatocytes: mechanisms and consequences for quantitative clearance prediction. Drug Metab Dispos. 2007;35(8):1325-32.

[21] de Klerk DJ, Honeywell RJ, Jansen G, Peters GJ. Transporter and Lysosomal Mediated (Multi)drug Resistance to Tyrosine Kinase Inhibitors and Potential Strategies to Overcome Resistance. Cancers (Basel). 2018;10(12).

[22] Krchniakova M, Skoda J, Neradil J, Chlapek P, Veselska R. Repurposing Tyrosine Kinase Inhibitors to Overcome Multidrug Resistance in Cancer: A Focus on Transporters and Lysosomal Sequestration. Int J Mol Sci. 2020;21(9).

[23] Peters SA. Physiologically-Based Pharmacokinetic (PBPK) Modeling and Simulations Principles, Methods, and Applications in the Pharmaceutical Industry. 1st ed. Hoboken: Wiley; 2012. Print.

[24] Rodgers T, Leahy D, Rowland M. Physiologically based pharmacokinetic modeling 1: predicting the tissue distribution of moderate-to-strong bases. J Pharm Sci. 2005;94(6):1259-76.

[25] Leeuwerik AF. Physiologically based pharmacokinetic modeling to predict PET image quality of 3 generations EGFR-TKIs in advanced stage non-small cell lung cancer patients [master's thesis]. Utrecht: Utrecht University; 2021. 27 p.

[26] R Foundation for Statistical Computing. R: A language and environment for statistical computing [Internet]. Available from: http://www.R-project.org/. [Accessed 15th April 2022]

[27] Wickham, H. (2009) ggplot2: elegant graphics for data analysis. Springer New York.

[28] Rodgers T, Rowland M. Physiologically based pharmacokinetic modelling 2: predicting the tissue distribution of acids, very weak bases, neutrals and zwitterions. J Pharm Sci. 2006;95(6):1238-57.

[29] Graham H, Walker M, Jones O, Yates J, Galetin A, Aarons L. Comparison of in-vivo and in-silico methods used for prediction of tissue: plasma partition coefficients in rat. J Pharm Pharmacol. 2012;64(3):383-96.

[30] Joly-Tonetti N, Ondet T, Monshouwer M, Stamatas GN. EGFR inhibitors switch keratinocytes from a proliferative to a differentiative phenotype affecting epidermal development and barrier function. BMC Cancer. 2021;21(1):5.

[31] Assmus F, Houston JB, Galetin A. Incorporation of lysosomal sequestration in the mechanistic model for prediction of tissue distribution of basic drugs. Eur J Pharm Sci. 2017;109:419-30.

[32] Schmitt MV, Reichel A, Liu X, Fricker G, Lienau P. Extension of the Mechanistic Tissue Distribution Model of Rodgers and Rowland by Systematic Incorporation of Lysosomal Trapping: Impact on Unbound Partition Coefficient and Volume of Distribution Predictions in the Rat. Drug Metab Dispos. 2021;49(1):53-61.

[33] de Araujo MEG, Liebscher G, Hess MW, Huber LA. Lysosomal size matters. Traffic. 2020;21(1):60-75.

[34] Liu L, Wang C, Li S, Bai H, Wang J. Tumor immune microenvironment in epidermal growth factor receptor-mutated non-small cell lung cancer before and after epidermal growth factor receptor tyrosine kinase inhibitor treatment: a narrative review. Transl Lung Cancer Res. 2021;10(9):3823-39.

[35] Herbst RS, Onn A, Sandler A. Angiogenesis and lung cancer: prognostic and therapeutic implications. J Clin Oncol. 2005;23(14):3243-56.

[36] Folkman J. Tumor angiogenesis: therapeutic implications. N Engl J Med. 1971;285(21):1182-6.

[37] Hirano T, Yasuda H, Tani T, Hamamoto J, Oashi A, Ishioka K, et al. In vitro modeling to determine mutation specificity of EGFR tyrosine kinase inhibitors against clinically relevant EGFR mutants in non-small-cell lung cancer. Oncotarget. 2015;6(36):38789-803.

[38] EMA. Giotrif (INN-Afatinib) European Public Assessment Report 2013. Available from: http://www.ema.europa.eu/docs/en_GB/document_library/EPAR_Public_assessment_report/human/004124/WC500202024.pdf [Accessed 15th April 2022]

[39] EMA. Tarceva (INN-erlotinib) Summary of Product Characteristics 2005 [Available from: https://www.ema.europa.eu/en/documents/product-information/tarceva-epar-product-information_en.pdf [Accessed 15th April 2022]

[40] EMA. Tagrisso (INN-Osimertinib) European Public Assessment Report 2015. Available from: https://www.ema.europa.eu/en/medicines/human/EPAR/tagrisso [Accessed 15th April 2022]

[41] Englinger B, Kallus S, Senkiv J, Heilos D, Gabler L, van Schoonhoven S, et al. Intrinsic fluorescence of the clinically approved multikinase inhibitor nintedanib reveals lysosomal sequestration as resistance mechanism in FGFR-driven lung cancer. J Exp Clin Cancer Res. 2017;36(1):122.

[42] Wind S, Schnell D, Ebner T, Freiwald M, Stopfer P. Clinical Pharmacokinetics and Pharmacodynamics of Afatinib. Clin Pharmacokinet. 2017;56(3):235-50.

[43] Amor D, Goutal S, Marie S, Caille F, Bauer M, Langer O, et al. Impact of rifampicin-inhibitable transport on the liver distribution and tissue kinetics of erlotinib assessed with PET imaging in rats. EJNMMI Res. 2018;8(1):81.

[44] Zsila F, Fitos I, Bencze G, Keri G, Orfi L. Determination of human serum alpha1-acid glycoprotein and albumin binding of various marketed and preclinical kinase inhibitors. Curr Med Chem. 2009;16(16):1964-77.

[45] Huang Z, Ung T. Effect of alpha-1-acid glycoprotein binding on pharmacokinetics and pharmacodynamics. Curr Drug Metab. 2013;14(2):226-38.

[46] Ling J, Johnson KA, Miao Z, Rakhit A, Pantze MP, Hamilton M, et al. Metabolism and excretion of erlotinib, a small molecule inhibitor of epidermal growth factor receptor tyrosine kinase, in healthy male volunteers. Drug Metab Dispos. 2006;34(3):420-6.

[47] Abuqayyas L, Balthasar JP. Application of PBPK modeling to predict monoclonal antibody disposition in plasma and tissues in mouse models of human colorectal cancer. J Pharmacokinet Pharmacodyn. 2012;39(6):683-710.

[48] Mamada H, Iwamoto K, Nomura Y, Uesawa Y. Predicting blood-to-plasma concentration ratios of drugs from chemical structures and volumes of distribution in humans. Mol Divers. 2021 Aug;25(3):1261-1270. doi: 10.1007/s11030-021-10186-7. Epub 2021 Feb 10. PMID: 33569705; PMCID: PMC8342319.

[49] Elmokadem A, Riggs MM, Baron KT. Quantitative Systems Pharmacology and Physiologically-Based Pharmacokinetic Modeling With mrgsolve: A Hands-On Tutorial. CPT Pharmacometrics Syst Pharmacol. 2019 Dec;8(12):883-893. doi: 10.1002/psp4.12467.

[50] Yang J, Jamei M, Yeo KR, Rostami-Hodjegan A, Tucker GT. Misuse of the well-stirred model of hepatic drug clearance. Drug Metab Dispos. 2007 Mar;35(3):501-2. doi: 10.1124/dmd.106.013359. PMID: 17325025.

[51] Williams JA, Ring BJ, Cantrell VE, Jones DR, Eckstein J, Ruterbories K, et al. Comparative metabolic capabilities of CYP3A4, CYP3A5, and CYP3A7. Drug Metab Dispos. 2002;30(8):883-91.

[52] Ward C, Meehan J, Gray ME, Murray AF, Argyle DJ, Kunkler IH, et al. The impact of tumour pH on cancer progression: strategies for clinical intervention. Explor Target Antitumor Ther. 2020;1:71-100. https://doi.org/10.37349/etat.2020.00005

Appendix

I: Histological analysis of vasculature

CD31 staining is widely used to quantify neovascularization since CD31 is abundantly found on the surface of endothelial cells. Quantitative evaluation of vascularization was performed by analysis of images (obtained from the Human Protein Atlas (www.proteinatlas.org) of immunohistochemical CD31 stainings of lung tissue. Microvessel density (MVD) was then determined by counting the number of vessels per tissue area. To obtain the vascularization coefficient, ratio of MVD was divided by the mean MVD of healthy tissue. The analysis included eight adenocarcinoma and four normal lung tissue samples. Mean MVD of tumor tissue was 85 (± 36) and for healthy tissue mean MVD was 237 (±74). The vasculature coefficient of NSCLC was therefore 85/237 = 0.36. **Supplemental figure 1** shows the MVD of all analyzed samples.

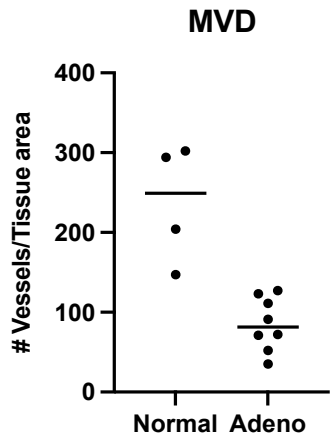

Supplemental figure 1: MVD of each sample. # =number of. Normal = healthy tissue. Adeno = adenocarcinoma, tumor tissue. MVD= micro vessel density

II: Whole-body distribution of EGFR-TKIs

The whole-body distribution of the three EGFR-TKIs was described by the mechanistic model. The predicted TBR values compared to the measured TBR (obtained during PET imaging).

Table 1: PET image derived tissue-to-blood ratios compared to predicted TBR in all tissues of interest. SD are given in brackets

	Erlotinib			**Afatinib**			**Osimertinib**		
	Predicted	Observed	*Prediction error (%)*	Predicted	Observed	*Prediction error (%)*	Predicted	Observed	*Prediction error(%)*
Brain	0.18	n.a.	n.a.	2.26	0.08 (0.03)	187.1	2.25	0.79 (0.5)	95.7
Lung	0.30	0.51 (0.2)	-52.6	5.47	2.54 (1.2)	73.3	4.60	7.01 (1.6)	-41.4
Spleen	0.18	1.46 (0.4)	-155.3	38.7	13.23 (2.3)	98.0	37.5	18.09 (7.7)	69.9
Kidney	0.23	1.69 (0.6)	-152.9	20.8	6.93 (1.8)	100.0	15.5	5.61 (2.0)	93.9
Bone	0.15	1.23 (0.2)	-155.7	2.16	4.81 (2.0)	-75.9	2.19	4.24 (0.7)	-63.8
Tumor	0.30	1.42 (0.5)	-129.6	12.1	3.60 (2.4)	108.4	3.42	5.60 (2.0)	-48.5